A General Approach for Quantifying the Benefit of Distributed Power Electronics for Fine Grained MPPT in Photovoltaic Applications Using 3-D Modeling

Shahab Poshtkouhi, *Student Member, IEEE*, Vishal Palaniappan, Miad Fard, and Olivier Trescases, *Member, IEEE*

Abstract—This paper deals with photovoltaic power installations in urban environments. A general simulation method is developed to quantify the total energy yield for photovoltaic (PV) installation sites exploiting different levels of Distributed Maximum Power Point Tracking (DMPPT) granularity. The process includes 3-D modeling, shading evaluation of the installation site, and irradiance calculations on the PV surfaces on an hourly basis throughout the year. Three leading microconverter topologies are analyzed and the cost/performance tradeoff is discussed for panel-level DMPPT. The energy yield evaluation technique is confirmed by means of several miniature PV acquisition units for frequent irradiance and temperature measurements in the installation site. The yearly energy yield benefit is shown to be highly dependent on the relative shading in the three installation sites. It is found that the energy yield benefit easily outweighs the power electronics costs in two of the three installations for panel-level DMPPT. The analysis method can be used by PV installers and system designers for accurate energy yield prediction, as well as power electronics engineers who need to bound the cost of their design based on the net energy benefit of the installed PV system.

Index Terms—DC–DC converter, distributed maximum power point tracking (DMPPT), partial shading, performance analysis, photovoltaic (PV) installation, solar energy, solar forecasting, 3-D modeling.

I. INTRODUCTION

THE GRADUAL reduction in the cost of photovoltaic (PV) panels, combined with favorable feed-in tariffs in a variety of countries, is leading to the rapid deployment of PV installations in urban settings. The energy yield of these small-scale, sub 10-kW installations is usually reduced by mismatches in the operating conditions of the individual PV cells, which are typically connected in series/parallel arrangements. The nonuniformity in operating conditions is caused by external factors such as clouds, reflections, partial shading, dirt, temperature gradients, or intrinsic factors such as semiconductor process variations and aging. PV panels having nonuniform irradiation and temperature cannot be operated at their respective maximum power point (MPP), since they are forced to operate with the same terminal voltage in parallel-connected systems or at the same string current in series-connected systems. Using power electronic converters for distributed maximum power point tracking (DMPPT) is well known to alleviate problems associated with mismatched panels [1]–[6].

The emergence of various startup companies and research efforts aimed at developing low-cost, high-efficiency microinverters and micro dc–dc converters (microconverters) for DMPPT has raised important questions about the true benefits of a distributed approach. The additional cumulative energy savings from DMPPT must be carefully weighed against the increased system cost and the potential for reduced mean-time-before-failure. While DMPPT hardware solutions are well covered in the literature and industry brochures, there is a need for a comprehensive analysis of DMPPT benefits for real-world PV installations.

One of the most important design considerations in a monocrystalline or multicrystalline DMPPT system is the level of granularity for deploying the power converters. Thin-film PV systems offer different granularity tradeoffs and are beyond the scope of this paper. A microconverter-based DMPPT system utilizing a central inverter is illustrated in Fig. 1. DC–DC microconverters are clearly more appropriate than microinverters at higher levels of granularity due to lower overhead cost. Microconverters are the main focus of this paper, while the general forecasting approach can also be used for microinverter systems, such as [7]. If the power converter losses are neglected, single-cell-level granularity provides the maximum possible energy from a PV system. An accurate system model is required to evaluate the yearly energy benefit versus the DMPPT granularity.

Several papers and commercial tools have attempted to address mismatch in PV installations. In [8], a MATLAB-based model has been developed to determine the individual *I–V* and *P–V* characteristics of panels in a large PV array for general conditions. Although this tool is useful to study the effects of partial shading and temperature variations in the system for different configurations, it does not consider the real location and topography in which the PV array is installed, and thus, it provides
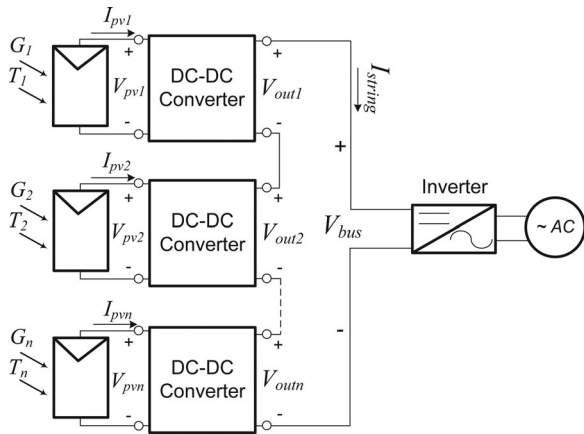
Fig. 1. Microconverter-based DMPPT architecture for series-connected PV systems.

limited insight into the true benefits of DMPPT. In [9], the total output energy for a certain residential installation is predicted by performing a site shade survey. This tedious task has limited accuracy, since the analysis is not automated and the data are limited to a finite number of days, from which the yearly shading must be estimated. In [10], a powerful method to estimate irradiance and shading from nearby obstacles on PV cells based on global irradiation data in the location of interest is introduced but the DMPPT design options and the power electronics interface are not discussed. In [11], the performance of DMPPT systems and the energy yield is investigated under extreme partial shading scenarios. In [12], the microconverters are accurately modeled for a series-connected PV system. Generic irradiation and temperature profiles of varying standard deviations are used to show that DMPPT can have a net detrimental impact on the energy yield in systems having near-uniform irradiance due to the additional power converter losses. In the commercial domain, several software packages such as PVcad [13] and PV-DesignPro [14] exist; however they mainly focus on modeling the PV array and do not consider complex partial shading conditions on the array in addition to neglecting the losses in the power converters [8].

This project has three main objectives.

1) Develop a general methodology to accurately forecast the hourly, monthly, and yearly energy yield of a specific PV installation for different levels of DMPPT granularity in the presence of localized, time-varying shading patterns.
2) Investigate the energy losses of the most popular PV microconverter topologies for panel-level DMPPT granularity in different installations having different shading conditions.
3) Develop an automated software package based on the two aforementioned objectives to help system designers and power electronics engineers evaluate and develop PV architectures.

This paper presents a versatile tool to investigate the effects of partial shading and nonideal power converter efficiency on the total harvested energy. The developed tool can shed more insight into the cost/benefit tradeoff of microconverter

topologies [15], [16] for the desired PV installation. Google Sketchup [17] is used as the core of this tool to model the installation site. Google Sketchup is a 3-D design software that is easy-to-use and can be linked to Google Earth to extract the geographical characteristics of a target location. After the model has been developed in this software, hourly shading patterns are generated and transferred to the MATLAB environment for postprocessing and evaluation. The DMPPT benefit for different levels of granularity and the power electronics converters in series-connected systems are then considered and studied in this environment with the objective of helping system and power electronics designers optimize the PV installation and lower the power harvesting costs.

This paper is organized as follows. Section II introduces the DMPPT modeling approach. Section III covers the procedure for three different residential PV installations and includes a detailed energy yield analysis in each case. Section IV discusses a practical approach to verify the designed simulation procedure and enhance its accuracy by considering other important factors in a PV installation. Finally, Section V concludes this paper.

II. SIMULATION PROCEDURE

The improvement in harvested energy is the main incentive for choosing deeper levels of DMPPT granularity for a PV installation. One of the main reasons of degradation in a system's performance is the partial shading effect. This effect is illustrated on a series-connected PV panel string in Fig. 2. By-pass diodes are introduced to clamp the negative voltage V_{pv}, in order to avoid dissipating excessive power when a shaded panel is forced to operate at a high string current I_{string}, as shown in Fig. 2(a) for Panel #3.

The extent to which a certain PV installation suffers from the partial shading effect depends on many factors that should be considered for a system design. The software package components are discussed in the following sections.

A. Installation Site 3-D Modeling and Sun Synthesis

A 3-D computer-aided design (CAD) tool is used to model the installation site, including the obstacles and structures that cause shading on the PV array throughout the year. Existing CAD tools such as 3-D Studio Max, Autodesk Maya, and Google Sketchup were considered for this study. Google Sketchup [17] was adopted since it is free and readily usable by the power electronics and PV community, in contrast to other CAD tools, which are more targeted to graphics design experts and architects. Google Sketchup can be linked to Google Earth in order to extract terrestrial and geographical characteristics of the location of interest. Sketchup is capable of modeling the exact sun beam direction and shadows in the installation area. Google Sketchup also offers a powerful scripting environment, Ruby [18].

The method for modeling the PV installation site and calculating the shade data consists of the following steps.

1) Create a 3-D model of the installation site using Sketchup. A basic site survey might be necessary to determine the relevant obstacles.
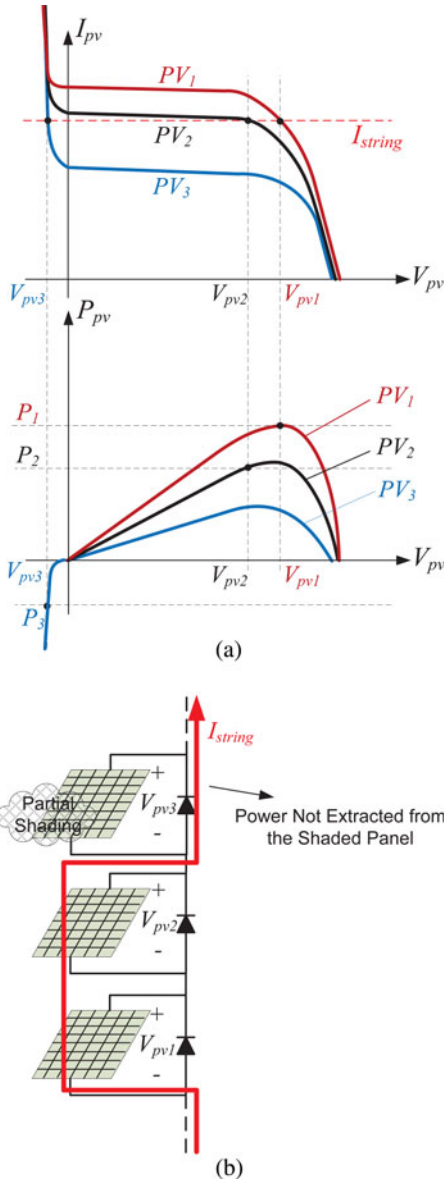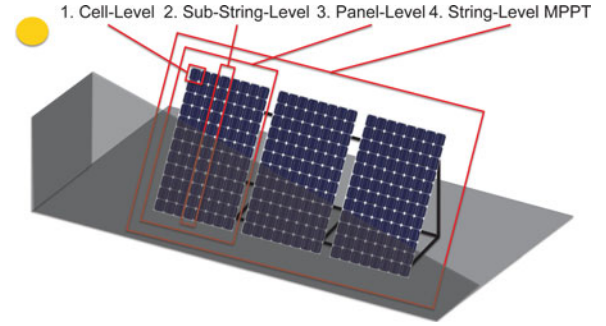
Fig. 3. Different potential granularity levels for performing DMPPT in the PV system.

B. Module Recognition

Today four levels of granularity are envisioned for monocrystalline PV, as illustrated in Fig. 3. The distributed power converter, either microconverter or microinverter, can be designed to achieve DMPPT at the 1) cell, 2) substring, 3) panel, and 4) string levels.

The choice of granularity clearly impacts the voltage/current ratings and cost of the power electronics. It is necessary to extract all the physical information about the potential DMPPT levels from the Sketchup model. The automated software package developed in this study includes a MATLAB script to locate all the individual cells, substrings, panels, and strings in the PV installation. An edge detection algorithm first recognizes all the closed-form patterns in the high-pass filtered image [19]. The use of high-pass filter is necessary so that the shade patterns are not identified mistakenly as PV cell boundaries. Each pattern's shape within the generated image is then identified accordingly. The PV cells can then be detected based on the their specific shape and gray scale in the constructed image, as depicted in Fig. 4. The image resolution is set such that X, the number of pixels on each side of the PV cell, is not less than 10 for accurate calculations. The module recognition unit sorts the recognized cells into substrings, panels, and strings and identifies them as groups based on the identified alignment and proximity of the PV cells in the image. The postprocessed graphical image for the installation site in Fig. 5(a) is shown in Fig. 5(b) with the recognized PV cells rendered in white.

C. PV Model

A monocrystalline silicon PV cell can be modeled by an equivalent circuit, as shown in Fig. 6(a) [20]. The output I–V characteristic is given by

$$I_{\mathrm{pv}} = I_{\mathrm{pv0}} - I_0 \left[\exp \left(\frac{V_{\mathrm{pv}} + R_s I_{\mathrm{pv}}}{V_t a} \right) - 1 \right] - \frac{V_{\mathrm{pv}} + R_s I_{\mathrm{pv}}}{R_p} \tag{1}$$

where I_{pv} and I_0 are the panel output and saturation currents, respectively. $V_t = N_s kT/q$ is the thermal voltage of the array with N_s cells in series and $p - n$ junction temperature T (in Kelvin). q is the electron charge, k is the Boltzmann constant, and a is the diode ideality constant. R_s and R_p are the equivalent series and parallel resistances of the PV cell. The light-generated

Fig. 2. Output power degradation due to partial shading in the series-connected PV string. (a) I–V and P–V characteristics of the series-connected panels. (b) Power loss due to by-pass diode conduction of the shaded panel.

2) A Ruby script is developed to set the viewing camera perpendicular to the PV panels' surface, adjust the date and time accordingly and synthesize the sun light and shadows using the sun tool. Ideally, the camera is set manually to cover all the PV panels in the installation area. However, it is possible to decompose the screen into several sub-sets to capture multiple images if the installation consists of a large number of panels, or if the panels cover a small portion with respect to the whole installation area.

3) The images are generated for each hour and saved in the desired resolution. Images are generated from 5 AM to 9 PM for each day, resulting in $17 \times 365 = 6205$ files.
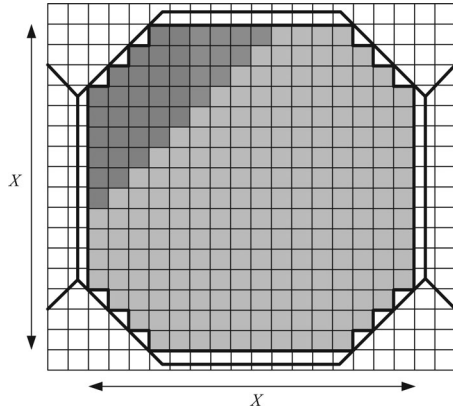
Fig. 4. PV cell's format in the constructed image of the installation site. X represents the number of pixels on each side of the PV cell, which depends on the resolution of the cell in the image.
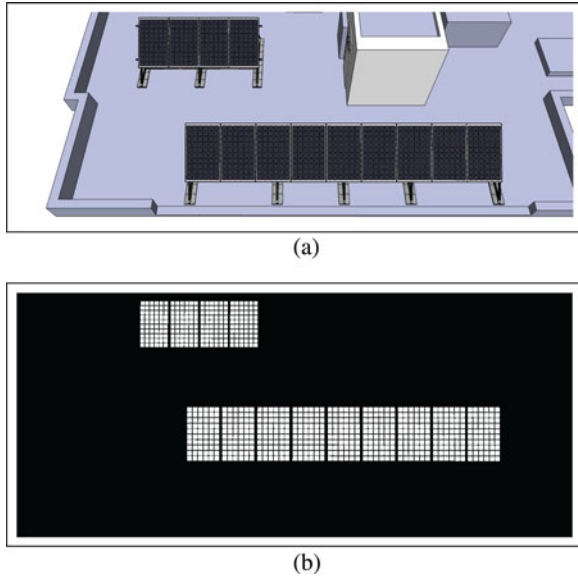

(a)

(b)

Fig. 5. (a) Original Sketchup model transferred to MATLAB for module recognition. (b) Recognized PV cells within the plane of panels.
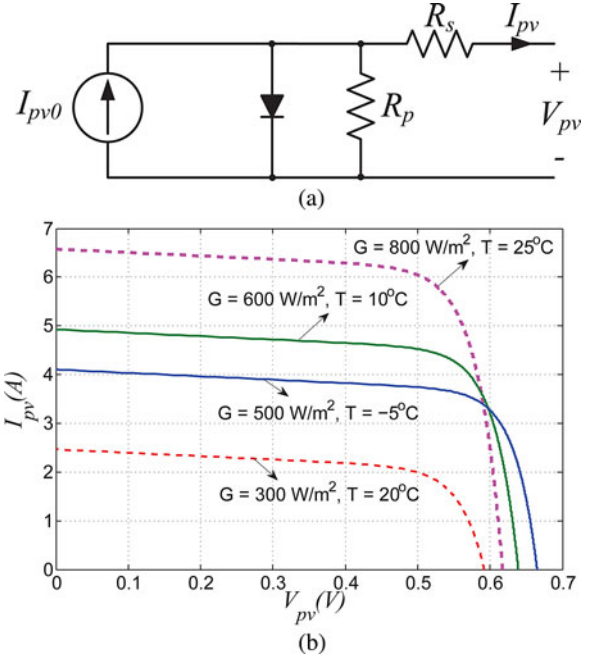

(a)

(b)

Fig. 6. (a) Equivalent circuit of a PV cell including the series and parallel resistances [20]. (b) Simulated I–V curves for different irradiation and temperature conditions.

TABLE I
PV CELL SPECIFICATIONS

Parameter	Specification	Unit
Nominal Short Circuit Current, I_{scn}	8.22	A
Nominal Open Circuit Voltage, V_{ocn}	0.627	V
Nominal Current at Max. Power, I_{mpn}	7.87	A
Nominal Voltage at Max. Power, V_{mpn}	0.51	V
Max. Power, P_{max}	4	W
Number of Series Cells in a Sub-string	10	
Number of Series Cells in a Panel	60	

current of the PV cell, I_{pv0}, depends on the total solar irradiation on the PV surface G_{tot} and temperature T according to [20]

$$I_{\mathrm{pv0}} = (I_{\mathrm{pvn}} + K_1 \Delta T) \frac{G_{\mathrm{tot}}}{G_n} \qquad (2)$$

where I_{pvn} is the light-generated current in nominal conditions which are usually $T_n = 25\ °C$ and $G_n = 1000\ \mathrm{W/m^2}$. Also, $\Delta T = T - T_n$ is the difference between the actual temperature T and the nominal temperature T_n. K_1 is the temperature coefficient of the PV current. G_{tot} represents the total sun irradiation on PV surface in $\mathrm{W/m^2}$.

The parameters of the monocrystalline PV cell considered for simulations in this paper are listed in Table I [21]. For this PV panel, $N_s = 1$ for a single cell, $N_s = 10$ for a substring, and $N_s = 60$ for the whole panel. The simulated I–V curves of this PV cell for various irradiation and temperature conditions are shown in Fig. 6(b). The I–V and P–V characteristics of the recognized substrings, panels, and strings are calculated based on the connection architecture and stored in the MATLAB environment.

D. Shading Evaluation and Power Estimation

The area of each PV cell in the hourly generated images is scanned to determine the percentage of shading across it as the sun moves across the sky. The percentage of shading S for a PV cell is calculated using

$$S = \frac{P_{ix,\mathrm{drk}}}{P_{ix,\mathrm{tot}}} \qquad (3)$$

where $P_{ix,\mathrm{tot}}$ and $P_{ix,\mathrm{drk}}$ represent the total number of pixels and the pixels with a higher gray scale code (shaded area) inside the PV cell boundary, respectively. The total irradiance on the PV panel surface G_{tot} can be decomposed into three portions [22]

$$G_{\mathrm{tot}} = G_r + G_d + G_b \qquad (4)$$

where the direct-normal irradiance G_r determines the incident irradiation hitting the surface directly from the sun, while the

indirect or diffuse sunlight coefficient G_d specifies the irradiation intensity caused by reflections and contributions of atmospheric steam and surrounding obstacles. The ground-reflected diffuse component G_b is the intensity of irradiance on the tilted surface due to the surrounding objects and ground albedo ρ.

The direct-normal irradiance G_r can be calculated from the horizontal global direct irradiance data $G_{r,\text{global}}$ by the following equation [23]:

$$G_r = G_{r,\text{global}} \cdot \cos i \qquad (5)$$

where i is the angle of the incident sun-beam on the PV surface and is defined by

$$\cos i = \cos \beta \cos z + \sin \beta \sin z \cos(\phi_s - \phi_{\text{pv}}) \qquad (6)$$

where β is the tilt angle of the panels, which is usually set according to the location's latitude for maximal performance [24], and ϕ_{pv} is the azimuth angle of the PV panels, which defines the deviation of the surfaces from the equator. If the PV panels are facing south, $\phi_{\text{pv}} = 180°$. ϕ_s is the azimuth angle of the sun and z is the zenith angle and has the following relationship with respect to location's latitude ϕ, solar declination angle δ, and hour-angle of the sun, ω:

$$\cos z = \sin \phi \sin \delta + \cos \phi \cos \delta \cos \omega. \qquad (7)$$

The hour-angle of the sun ω is calculated at the mid-hour for each hour h in the generated data set by

$$\omega = 15° \cdot h + 0.5 - 12. \qquad (8)$$

If the sky is considered isotropic, shading will not remove the diffuse portion of the incident irradiance. Thus, G_d can be set to the diffuse irradiance hitting a horizontal planar surface. This assumption has been considered in many models [25], [26]. However, the diffuse irradiance depends on many factors such as the geographic position, time and day of the year, level of clearness, humidity, altitude, and climate. For this reason, other diffuse irradiance estimation methods have been developed which categorize the diffuse irradiance into circumsolar, horizon brightening, and isotropic components [10], [22], [27]. If these models are used, shading will only keep the isotropic component of the total diffuse irradiance. The isotropic diffuse model has been used in this paper; however, the methodology can be easily applied to other diffuse light estimation methods.

The contribution of the ground-reflected diffuse component G_b is usually small and is given by

$$G_b = (1 - \cos \beta) G_{r,\text{global}} \frac{\rho}{2} \qquad (9)$$

where the ground-reflected coefficient ρ is a value between 0 and 1. In this paper, a constant albedo value of $\rho = 0.2$ is used.

A PV cell with S percentage of shading, total sun irradiance of G_{tot} and a diffuse sun irradiance of G_d can be characterized by finding I_{pv} from

$$I_{\text{pv}} = (1 - S) \cdot I_{\text{pv,tot}} + S \cdot I_{\text{pv},d} \qquad (10)$$

where $I_{\text{pv,tot}}$ and $I_{\text{pv},d}$ are the panel currents at the total and diffuse radiations, respectively, which can be found by evaluating the I–V curve for the corresponding voltage V_{pv} across the cell.

The I–V curve of each cell is obtained after it has been analyzed at each hour throughout the year based on its corresponding Sketchup image. The I–V characteristics and power points of the series connected cells in a sub-string, panel or string are then evaluated for different levels of granularity by combining the individual cells' obtained characteristics in the appropriate configuration.

E. Microconverter Topologies for DMPPT

The nonisolated dc–dc converters in Fig. 1 can be realized with a variety of topologies. For hard-switching converters, the buck–boost, boost–buck, and boost topologies are the most popular choices [1], [28]. The buck–boost and boost–buck topologies have the distinct advantage that they can theoretically guarantee that each input PV operates at the MPP for any value of I_{string}, as these converters can be operated in either boost, buck or pass-through mode [1]. In pass-through mode, the switches are set to connect V_{pv} directly to V_{out}. The switching losses are, therefore, eliminated and $V_{\text{out}} = V_{\text{pv}}$. The boost converter has a higher efficiency, lower cost, and reduced complexity compared to the four-switch topologies.

The three topologies of Fig. 7 were designed using commercially available components in order to explore cost and energy yield tradeoffs for panel-level MPPT, which dominates the market today. The design procedure for other levels of granularity obeys the same rules and thus is not covered in this paper. In each case, suitable devices from Infineon Technologies are chosen based on the converter requirements. The specifications and total cost for the chosen components are listed in Table III. The total microconverter cost is substantially higher due to the need for control and auxiliary power ICs. The inductors for all microconverters are chosen from the same manufacturer (Vishay) and the inductances, L_1 and L_2, are selected to achieve the same relative ripple, $\frac{\Delta i_L}{I_L}$ at the rated output power. The input and output capacitors, C_{in} and C_{out}, are sized to achieve the same input and output voltage ripple in the three topologies. The most expensive parts of each converter are the ceramic output capacitors due to the high output voltage ratings as well as substantial capacitance needed for operation in boost mode. The ratio of active to passive component cost is provided in Table III.

The efficiency of each microconverter is calculated at every operating point, based on the switching and conduction losses in the power-stage, similar to [12]. The efficiency of the three designed converters versus I_{string} is shown in Fig. 8 for a fixed irradiance of 400 W/m². As long as the panel operates at the MPP, it behaves as a constant power source. The converters automatically change their operating modes depending on the relationship between the input and output current, as outlined in [1]. The highest efficiency is achieved in pass-through mode, where $I_{\text{string}} = I_{\text{pv}}$. The duty cycle in the boost converter saturates for $I_{\text{string}} > I_{\text{pv}}$, which causes the panel to operate away from the MPP.

In the general analysis presented in the following section, the operating point, mode, and efficiency for each microconverter are determined for each shading pattern, which are generated hourly. It is assumed that the dc-bus voltage V_{bus} is regulated
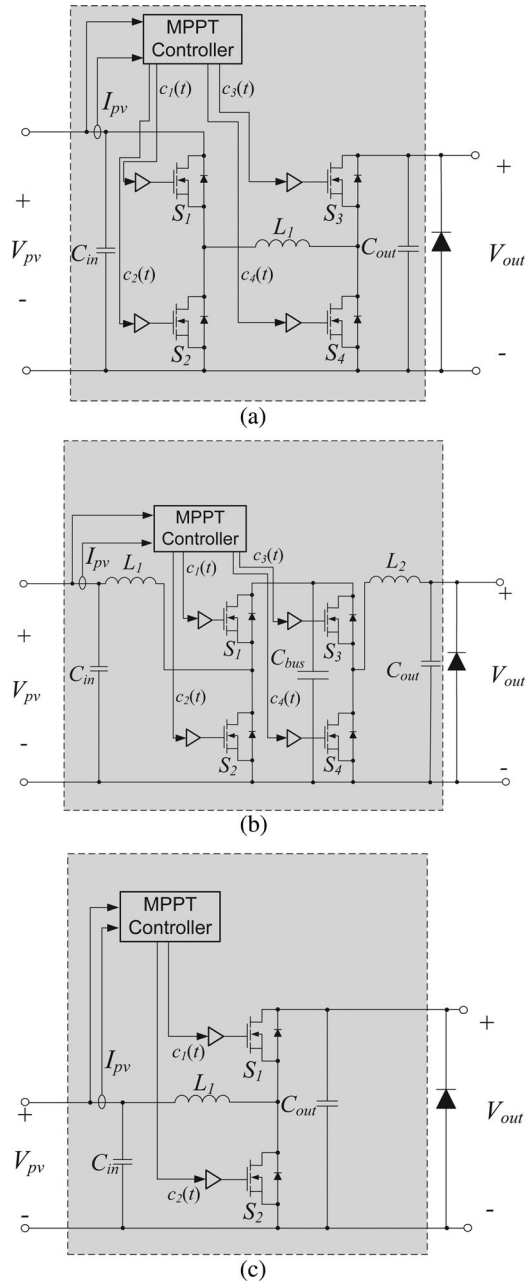
(a)

(b)

(c)

Fig. 7. Three popular hard-switching microconverter topologies in PV systems: (a) buck–boost, (b) boost–buck, and (c) boost.

Fig. 8. Buck–boost, boost–buck, and boost converters' efficiencies for $G_{\text{tot}} = 400$ W/m^2 and $T = 25\ ^\circ$C.

(a)

(b)

(c)
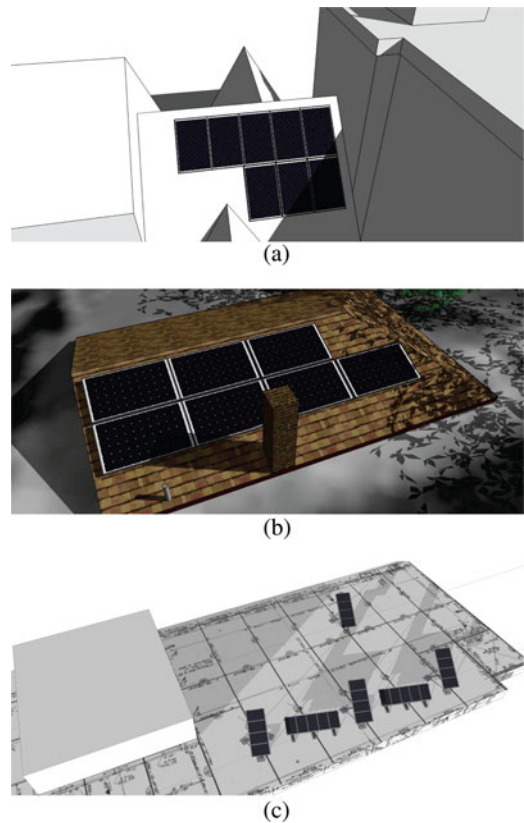
Fig. 9. Sketchup models for the PV installation at (a) Site #1, (b) Site #2, and (c) Site #3.

by the central inverter of Fig. 1 through the control of I_{string} [1]. The value of V_{bus}, therefore, has a strong impact on the microconverter efficiency.

III. CASE STUDIES AND SIMULATION RESULTS

Three urban PV installation sites were analyzed using the proposed forecasting software. Fig. 9 shows 3-D Sketchup models of the three installation sites in Toronto area. The simulation process described in Section II is used to determine the effectiveness of DMPPT in these installation sites. Important characteristics of each site are listed in Table II, including the relative extent
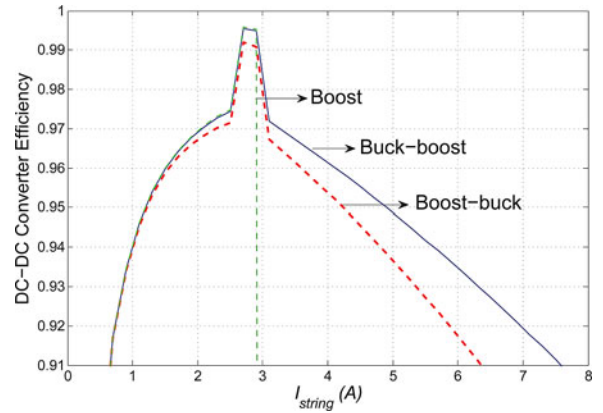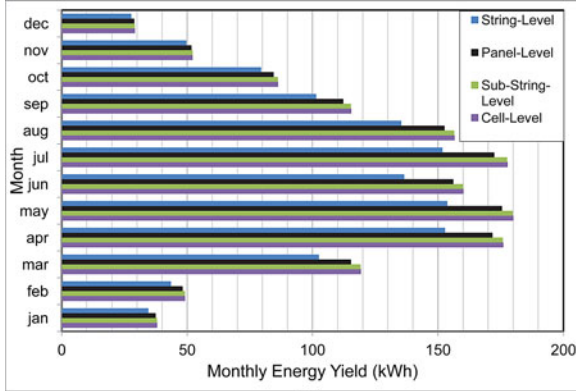
of shading and obstacles. Site #3 is located at the University of Toronto and was installed in 2011.

A. Total Energy Yield for Different Levels of DMPPT Granularity
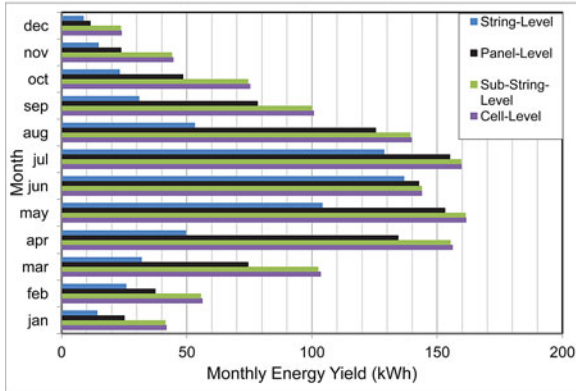
The simulation method described in Section II is used to estimate the total yearly energy yield in each site for different levels of DMPPT granularity. Irradiation and ambient temperature data from the University of Toronto's meteorological station from November 2009 to October 2010 is used for the energy
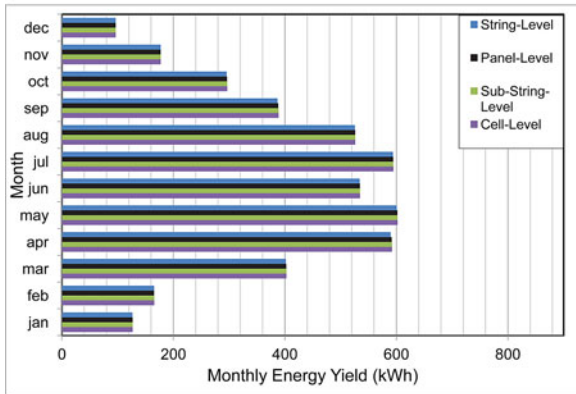
TABLE II
PV INSTALLATION SITES CHARACTERISTICS

Site #	Relative Shading	Main Obstacles	Building Type	Number of Panels	Power (kW)
1	Medium	Tall obstructions nearby	Residential	8	1.92
2	High	Trees and tall chimney	Residential	7	1.68
3	Low	PV racks	Commercial (UofT)	26	6.24

(a)

(b)

(c)

Fig. 10. Simulated annual energy yield for (a) Site #1, (b) Site #2, and (c) Site #3. The energy bars for each month are plotted in descending order of granularity.

TABLE III
MICROCONVERTER COMPONENT SPECIFICATIONS†

Component	Buck-boost	Boost-buck	Boost	Units
L_1	33	15	15	μH
L_2		33		μH
C_{in}	40	40	10	μF
C_{out}	18.4	18.4	18.4	μF
$R_{on}(S_{1,2})$	6	6	32	mΩ
$R_{on}(S_{3,4})$	32	32		mΩ
Normalized Power-Stage Cost	7.5	8.58	7.12	¢/W$_p$
Passive/Active Cost Ratio	3.4	4.1	4.5	

†A switching frequency of $f_s = 250$ kHz is used for all designs. For the boost–buck topology, $C_{\text{bus}} = 18$ μF. The power-stage cost estimate is based on Digikey prices and normalized to 240 W.

TABLE IV
RELATIVE ENERGY YIELD SAVINGS VERSUS DMPPT GRANULARITY

Site #	DMPPT			
	Cell-level B_4 (%)	Sub-string-level B_3 (%)	Panel-level B_2 (%)	String-level B_1 (%)
1	14.6	14.5	11.8	0
2	94.0	93.0	62.3	0
3	0.2	0.2	0.17	0

thermal model for the PV. For simplicity, T is considered to be always 5 °C higher than the ambient temperature T_a in this study. The resulting energy yield for the three test sites is shown in Fig. 10. The results confirm that the presence of obstacles in Site #2 makes the energy yield highly sensitive to the level of DMPPT granularity. On the other hand, using cell-level DMPPT rather than sub-string-level DMPPT might not be justified, due to the added complexity, cost, and reliability issues in addition to limited yield benefits. For Site #1, which is relatively free of obstacles, there is a substantial benefit for panel-level DMPPT over the string-level DMPPT, while the benefits for deeper granularity levels are not easily justified. For Site #3, which is nearly unobstructed, utilizing conventional series-connected PV architectures with by-pass diodes and a central inverter is recommended. The energy yield results for the three test cases are summarized in Table IV. The percentage improvement in the energy yield, B_n for the nth level of granularity is defined by

$$B_n = \frac{(E_n - E_1)}{E_1} \cdot 100\% \tag{11}$$

where E_1 is the energy yield for string-level DMPPT, which is used as a reference ($B_1 = 0$) and E_n is the energy yield for the

estimations [29]. This database contains the global irradiation $G_{r,\text{global}}$, as well as the temperature recordings of the year. Using this information, the total irradiation on the PV surface G_{tot} can be determined from (5) and (9). Furthermore, the junction temperature T can be estimated by considering an equivalent
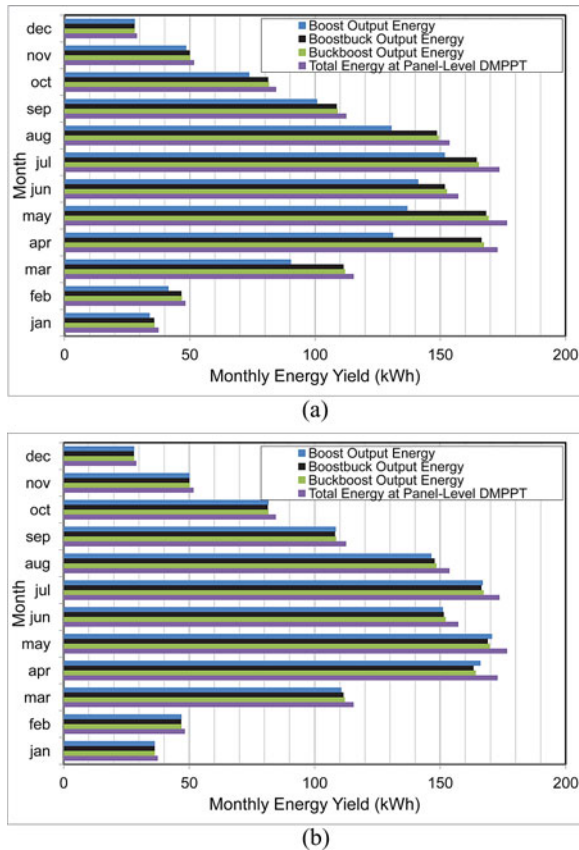
Fig. 11. Simulated energy yield at the dc–dc converter output for the eight-panel series-connected string in Site #1 for (a) $V_{\mathrm{bus}} = 230$ V and (b) $V_{\mathrm{bus}} = 280$ V.

nth level of granularity, where $n = 4$ corresponds to cell-level DMPPT.

B. Effect of Microconverters for Panel-Level DMPPT

The following analysis deals exclusively with panel-level DMPPT. The shading data were combined with the microconverter loss models to evaluate competing microconverters for several regulated values of V_{bus}. The total energy yield of Site #1 with all the panels in series and two different inverter bus voltages is shown in Fig. 11. The boost microconverter yields 0.3% more energy than boost–buck microconverter for $V_{\mathrm{bus}} = 280$ V due to its higher efficiency, despite the fact that the boost converter is unable to maintain MPPT under all shading conditions. The boost microconverter loses its advantage for $V_{\mathrm{bus}} = 230$ V since the duty-cycle saturation often forces the shaded panels to operated away from the MPP.

For the lower bus voltage of $V_{\mathrm{bus}} = 230$ V, the total output energy in the system for buck–boost and boost–buck microconverters is improved by roughly 0.2% due to the increased time spent in pass-through and buck modes. For the boost microconverter, decreasing V_{bus} reduces the output harvested power significantly, mainly because the by-pass diodes are turned ON more often.

Table V lists the percentage of time spent in boost, buck, pass-through events between 5 AM and 9 PM, for the buck–boost

TABLE V
PERCENTAGE OF TIME SPENT IN EACH MODE FOR BUCK–BOOST MICROCONVERTER FOR SITE #1

V_{bus}	Operating Mode		
	Boost (%)	Buck (%)	Pass-through (%)
208 V	62.5	31.0	6.5
230 V	73.3	19.7	7
330 V	97.9	1.0	1.1
500 V	98.3	0.7	0.9

TABLE VI
AGGREGATE EFFICIENCY η_a OF DIFFERENT MICROCONVERTERS FOR SITE #1

V_{bus}	Micro-Converter		
	Boost (%)	Boost-Buck (%)	Buck-Boost (%)
208 V	60.8	96.1	96.7
230 V	84.5	96.1	96.6
330 V	95.3	95.1	95.6
500 V	92.0	91.9	92.3

microconverter throughout the year and for four values of V_{bus} in Site #1. The mode distribution of boost–buck microconverter is nearly identical to the buck–boost microconverter and is omitted from the figure. For each value of V_{bus}, the by-pass diodes turn ON for less then 0.1% of the time slots.

Finally, the yearly aggregate efficiency η_a of three microconverters is given in Table VI for Site #1. The aggregate efficiency η_a is given by

$$\eta_a = \frac{\sum_{\mathrm{year}} V_{\mathrm{bus}} I_{\mathrm{string}}}{\sum_{\mathrm{year}} \sum_{i=1}^{M} V_{\mathrm{mpi}} I_{\mathrm{mpi}}} \quad (12)$$

where M is the number of panels in the installation and V_{mpi} and I_{mpi} are the operating voltage and current of the ith panel in its MPP. The aggregate efficiency obtained from the method presented in this paper is an accurate way to predict the relative performance of competing microconverters. The results show that if V_{bus} is properly optimized, η_a for the boost microconverter is competitive with the other topologies, while offering lower cost, size, and complexity.

It is informative to combine the results of Table IV and V. If we assume $\eta_a = 95\%$, the yield benefit from adding microconverters to achieve panel-level DMPPT instead of string-level MPPT reduces from 11.8% to 6.2% in Site #1. Using microconverters with the same η_a would decrease the benefit from 62.3% to 54.2% in Site #2, while a net loss of 5% would be expected in Site #3. Assuming a cost of $2/W_p$ for PV panels, the microconverters provide a net benefit as long as the incremental cost is below $0.12/W_p$ and $0.9/W_p$ for Site #1 and #2, respectively, which is in agreement with Table III . Clearly, the cost of other components and installation of the microconverters must also be included. The analysis can be repeated for any level of granularity and power converter specifications.

The simulated operation of the buck–boost microconverter system in Site #1 is shown in Fig. 12 for three consecutive days beginning from May 10, 2010 with $V_{\mathrm{bus}} = 208$ V. The hourly average irradiance on the PV surfaces, $G_{\mathrm{tot,ave}}$, and total output power for panel-level DMPPT are shown in Fig. 12(a) and (b),
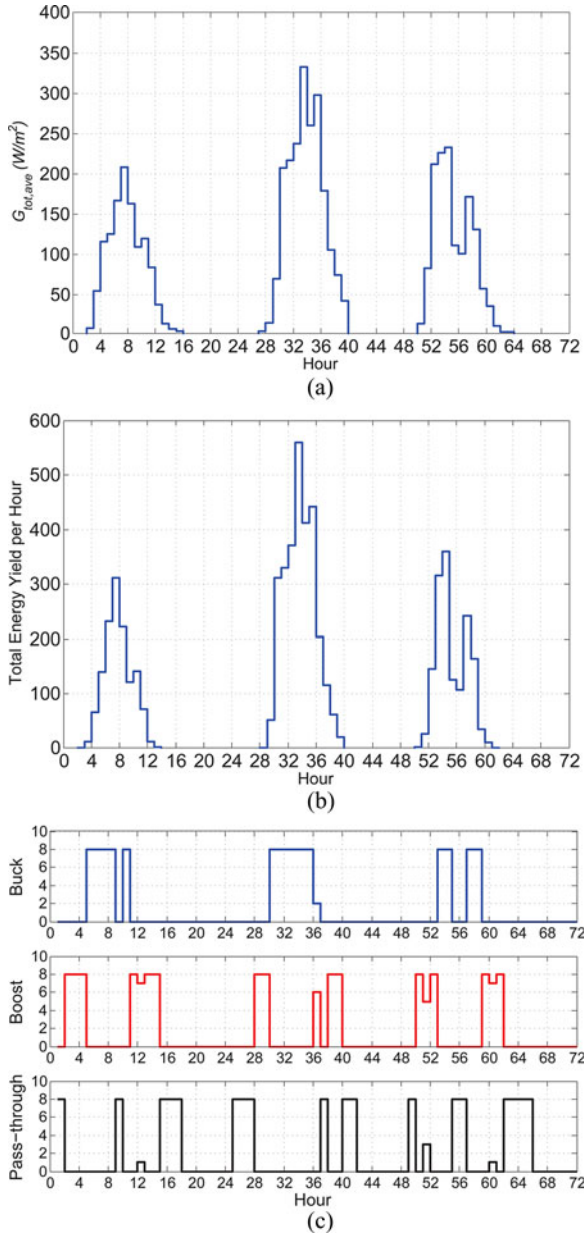
Fig. 12. Simulated working operation for May 10–12, 2010 (total of 72 h) in Site #1 for $V_{\mathrm{bus}} = 208$ V. (a) Total average calculated irradiance on tilted PV surfaces, $G_{\mathrm{tot,ave}}$. (b) Total energy yield per hour at panel-level for the PV installation. (c) Number of microconverters operating in buck, boost, and pass-through mode in each hour.
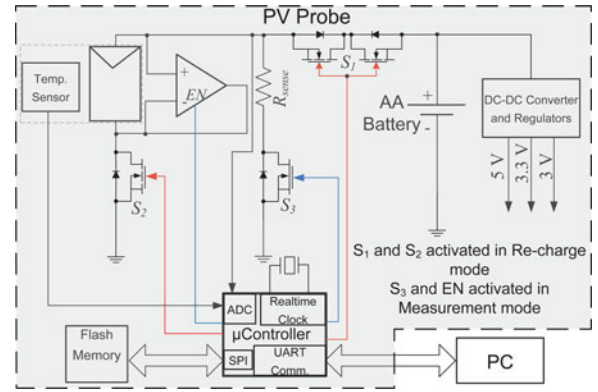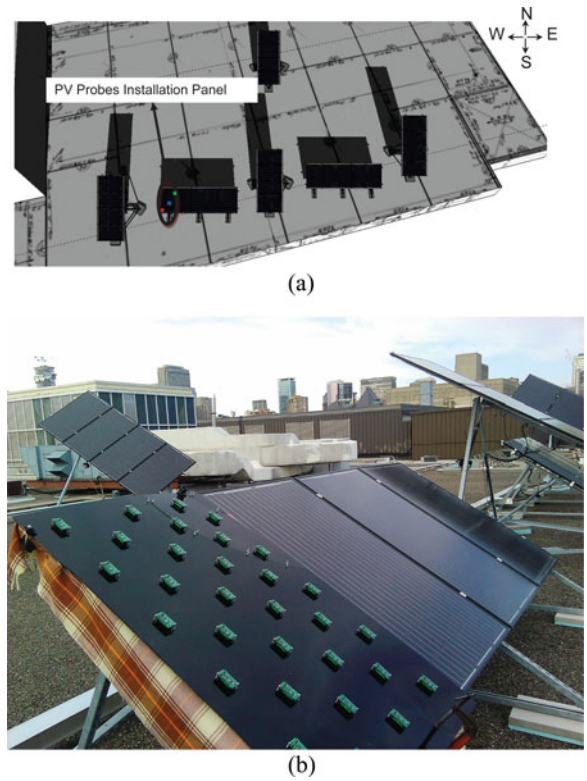

Fig. 13. PV probe architecture.

Fig. 14. (a) Installation location of the PV probes with the east, west, and middle-side probes indicated. (b) PV probe setup for installation site #3.

respectively. Fig. 12(c) shows the number of microconverters operating in buck, boost, and pass-through mode in each hour for the eight panel system. In general, as G_{tot} increases, the pass-through and buck mode occurrences increase due to the increase in the operating voltages of the panels.

IV. SHADE PATTERN MEASUREMENTS

Miniature stand-alone sensor modules (PV probes) were built to experimentally measure irradiance and temperature profiles on Site #3, in order to validate the modeling approach introduced in this paper. The PV probe architecture is shown in

Fig. 13. Each PV Probe is completely autonomous and includes a miniature monocrystalline PV cell [30], a temperature sensor, power management circuits, a microcontroller, and a flash memory module. The PV probe has two operating modes: 1) recharge and 2) data acquisition. During the recharge mode, switches S_1 and S_2 are turned ON, while the op-amp is driven to tristate mode and S_3 is turned OFF. In this mode, the 18-mW PV cell recharges the single AA battery. Once every 5 s, the PV probe short-circuits the panel using S_3 and measures the ambient temperature, T_a, and the short circuit current I_{sc}, through the precision sense resistor R_{sense}. The sampled T_a and I_{sc} are saved in a nonvolatile Flash memory before returning to recharge mode.
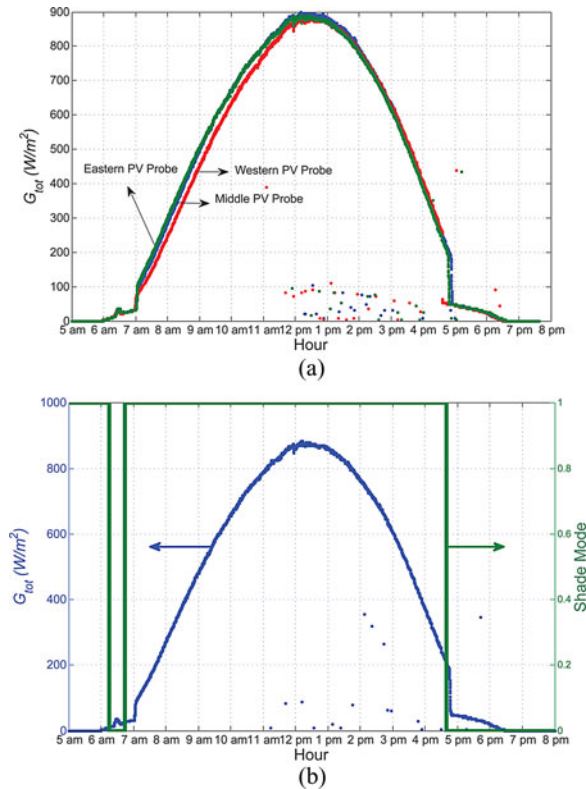
Fig. 15.   Calculated irradiance G_{tot} on the PV surfaces based on measured I_{sc} and T_a for (a) three PV probes and (b) one of the PV probes and the shading mode of the corresponding cell in Google Sketchup for different times of the day on May 9, 2011 (Shade mode = 0 means there is shading on the cell).

V. Conclusion

This is one of the first research efforts to combine a detailed analysis of 3-D shading patterns on PV installations and distributed power electronic converters of varying granularity having nonideal efficiency. The results of this study should help to shed light on the true value of distributed MPPT. It was found that the yearly energy yield was highly dependent on the relative shading in the three installations considered in this study. Panel and substring-level DMPPT generally appear to be the appropriate levels of granularity for urban environments, depending on the shading conditions. The benefits of cell-level DMPPT is very limited, unless there is a strong variation in the PV cell parameters, which can also be readily investigated with the proposed technique. It was found that the energy yield benefit for panel-level DMPPT easily outweighs the power electronics costs in two of the three installations, which is encouraging for the many companies and researchers working toward microconverter and microinverter hardware solutions. The impact of the distributed power electronics on system reliability and control remains one of the major issues to be addressed. The analysis method can be used by PV installers for accurate yield prediction, as well as power electronics engineers who need to bound the cost of their design based on the net energy benefit of their DMPPT system. The full software package developed in this paper, is available online [31].

The simulation process, including 3-D modeling and irradiation estimation, is validated using PV probes for one of the test sites considered in this paper. These low-cost PV probes can also be used to investigate nonsystematic shading.

Thirty PV Probes were installed in a checker-board pattern on one of the PV panel locations shown in Fig. 14(a) in Site #3. Each individual PV cell's irradiation and ambient temperature can be approximated by averaging its four adjacent recorded values. Fig. 15(a) shows the total solar irradiance on the tilted surface for a sunny day, calculated by extracting I_{sc} and T_a from three PV probes at the east, west, and middle-side of the panel. As expected, there is a clear time shift in the irradiation at different PV probe locations. The experimental curves have high-frequency variations due to nonsystematic shading from nonstationary obstacles such as clouds. This introduces another potential application of the PV probes, since they can be used as to quantify the nonsystematic shading for a certain installation location.

Fig. 15(b) shows the irradiation curve for one of the PV probes on the panel. There are two major shading occurrences in Site #3, at dusk and dawn. The shade mode bit represents the shading condition on the corresponding cell, based on the Google Sketchup 3-D model and is set to zero if the cell is partially shaded. The two measured shading events are properly predicted by the model. The slight time offset is systematic and can be attributed to the probe positioning and has a negligible effect on the energy yield results.

References

[1] L. Linares, R. Erickson, S. MacAlpine, and M. Brandemuehl, "Improved energy capture in series string photovoltaics via smart distributed power electronics," in *Proc. IEEE Appl. Power Electron. Conf. Expo.*, 2009, pp. 904–910.

[2] G. Walker, J. Xue, and P. Sernia, "PV string per-module maximum power point enabling converters," presented at the Proc. Australasian Univ. Power Eng. Conf., Christchurch, New Zealand, 2003.

[3] G. Walker and J. Pierce, "Photovoltaic DC–DC module integrated converter for novel cascaded and bypass grid connection topologies—Design and optimization," in *Proc. IEEE Power Electron. Spec. Conf.*, 2006, pp. 1–7.

[4] S. Bibian and H. Jin, "Cascaded dc–dc converter connection of photovoltaic modules," *IEEE Trans. Power Electron.*, vol. 19, no. 4, pp. 1130–1139, Jul. 2004.

[5] N. Femia, G. Lisi, G. Petrone, G. Spagnuolo, and M. Vitelli, "Distributed maximum power point tracking of photovoltaic arrays: Novel approach and system analysis," *IEEE Trans. Ind. Electron.*, vol. 55, no. 7, pp. 2610–2621, Jul. 2008.

[6] E. Roman, R. Alonso, P. Ibanez, S. Elorduizapatarietxe, and D. Goitia, "Intelligent PV module for grid-connected PV systems," *IEEE Trans. Ind. Electron.*, vol. 53, no. 4, pp. 1066–1073, Jun. 2006.

[7] Y. Fang and X. Ma, "A novel PV microinverter with coupled inductors and double-boost topology," *IEEE Trans. Power Electron.*, vol. 25, no. 12, pp. 3139–3147, Dec. 2010.

[8] H. Patel and V. Agarwal, "MATLAB-based modeling to study the effects of partial shading on PV array characteristics," *IEEE Trans. Energy Convers.*, vol. 23, no. 1, pp. 302–310, Mar. 2008.

[9] C. Deline, "Partially shaded operation of multi-string photovoltaic systems," in *Proc. IEEE Photovoltaic Spec. Conf.*, 2010, pp. 394–399.

[10] M. Drif, P. J. Perez, J. Aguilera, and J. D. Aguilar, "A new estimation method of irradiance on a partially shaded PV generator in grid-connected photovoltaic systems," *Renewable Energy*, vol. 33, no. 9, pp. 2048–2056, 2008.

[11] A. Bratcu, I. Munteanu, S. Bacha, D. Picault, and B. Raison, "Cascaded dc–dc converter photovoltaic systems: Power optimization issues," *IEEE Trans. Ind. Electron.*, vol. 58, no. 2, pp. 403–411, Feb. 2011.

[12] S. Poshtkouhi, J. Varley, R. Popuri, and O. Trescases, "Analysis of distributed peak power tracking in photovoltaic systems," in *Proc. IEEE Int. Power Electron. Conf.*, 2010, pp. 942–947.

[13] PVCad [software]. Fraunhofer-Inst. Wind Energy and Energy System Technol. (2007). [Online]. Available: http://www.iset.uni-kassel.de

[14] PV-DesignPro [software]. Maui Solar Energy Softw. Corp. (2006). [Online]. Available: http://www.mauisolarsoftware.com

[15] B. Liu, S. Duan, and T. Cai, "Photovoltaic dc-building-module-based BIPV system concept and design considerations," *IEEE Trans. Power Electron.*, vol. 26, no. 5, pp. 1418–1429, May 2011.

[16] Z. Liang, R. Guo, J. Li, and A. Huang, "A high-efficiency PV module-integrated dc/dc converter for PV energy harvest in FREEDM systems," *IEEE Trans. Power Electron.*, vol. 26, no. 3, pp. 897–909, Mar. 2011.

[17] (2008). Google Sketchup (Version 8.0.3117) [software]. Google Inc., [Online]. Available: http://sketchup.google.com/intl/en/download/

[18] Ruby [software]. Ruby Official Website. (2010). [Online]. Available: http://www.ruby-lang.org/en/downloads/

[19] A. Oppenheim, A. Willsky, and S. Hamid, *Signals and Systems*, 2nd ed. Englewood Cliffs, NJ: Prentice-Hall, 1997.

[20] M. Villalva, J. Gazoli, and E. Filho, "Comprehensive approach to modeling and simulation of photovoltaic arrays," *IEEE Trans. Power Electron.*, vol. 24, no. 5, pp. 1198–1208, May 2009.

[21] (2010). SW 240 mono. Solarworld Corp. Datasheet. [Online]. Available: http://www.solarworld-usa.com/solar-for-business-and-government/products-and-services/sunmodule-solar-panels.aspx

[22] M. Iqbal, *An Introduction to Solar Radiation*. Quebec, Canada: Academic, 1983.

[23] K. Y. Kondratyev, "Radiation regime of inclined surfaces," World Meteorol. Org., Geneva, Switzerland, Tech. Note 467, 1977.

[24] G. Lewis, "Optimum tilt of solar collector," *Solar Wind Energy*, vol. 4, pp. 407–410, 1987.

[25] B. Liu and R. Jordan, "Daily insolation on surfaces tilted towards the equator," *Trans. ASHRAE*, vol. 67, pp. 526–541, 1962.

[26] J. Jimenez and Y. Castro, National Assembly of Geophysics and Geodesy, vol. 2, 1986, p. 805. Available: http://ieeexplore.ieee.org/stamp/stamp.jsp?arnumber=04150472, reference [16].

[27] G. Notton, P. Poggi, and C. Cristofari, "Predicting hourly solar irradiations on inclined surfaces based on the horizontal measurements: Performances of the association of well-known mathematical models," *Energy Convers. Manage.*, vol. 47, pp. 1816–1829, 2006.

[28] R. K. Hester, C. Thornton, S. Dhople, Z. Zhao, and N. Sridhar, D. Freeman, "High efficiency wide load range buck/boost/bridge photovoltaic microconverter," in *Proc. IEEE Appl. Power Electron. Conf. Expo.*, 2011, pp. 309–313.

[29] UTM Meteorological Station. Univ. Toronto Dept. Geography, Mississauga, Canada. (2011). [Online]. Available: http://www.utm.utoronto.ca/7119.0.html

[30] IXOLAR High Efficiency SolarBIT. IXYS Datasheet. (2008). [Online]. Available: http://ixdev.ixys.com/DataSheet/

[31] (2011). PV Energy Estimation [software]. [Online]. Available: http://ele.utoronto.ca/~ot/projects/past_projects/PV/Energy_estimation.html

Vishal Palaniappan is currently working toward the Undergraduate in electrical and computer engineering at the University of Toronto, Toronto, ON, Canada.

He has been with Prof. Trescases' group since 2009, involved in multiple projects, including PV systems and electric vehicles.

Miad Fard is currently working toward the Undergraduate in electrical engineering, with core studies in power and electronics at the University of Toronto, Toronto, ON, Canada.

He has been an Undergraduate Researcher in Prof. Trescases' group since May 2010, involved in multiple projects such as photovoltaics, and educational development boards. As of October 2011, he is an intern at V Semiconductor Inc. as an Analog Design Engineer.

Olivier Trescases (M'01) received the Master and Doctoral degrees from the University of Toronto, Toronto, ON, Canada, in 2004 and 2007, respectively.

His Ph.D. dissertation was focused on high-efficiency, digitally controlled integrated switched-mode power supplies for portable applications. From 2007 to 2009, he was a Concept Engineer and Mixed-Signal Circuit Designer at Infineon Technologies AG, Villach, Austria. While at Infineon, he designed application-specific ICs in BCD (Bipolar/CMOS/DMOS) technologies for safety-critical automotive applications, such as electronic control units for airbag modules. He is the Co-Inventor of three patents. He joined the Department of Electrical and Computer Engineering, University of Toronto as an Assistant Professor in January 2009. His group conducts research on power electronics for automotive, industrial, aerospace and photovoltaic applications. He is currently involved in a number of research projects dealing with distributed maximum power point tracking for PV applications, power converters for high-brightness LEDs, battery management circuits for electric vehicles, integrated dc–dc converters, and high-frequency digital control schemes.

Dr. Trescases received the Charitat Award from the IEEE International Symposium on Power Semiconductor Devices and ICs in 2006 and the IEEE Hackbush Award in 2002. In 2010, he was a Co-Recipient of the Green Innovation Award from the City of Toronto. He is a member of the executive committee for the IEEE Toronto Section.

Shahab Poshtkouhi (S'10) received the B.A.Sc. degree in electrical engineering from Sharif University of Technology, Tehran, Iran, in 2009, and the M.A.Sc. degree in electrical engineering from the University of Toronto, Toronto, ON, Canada in 2011, where he is currently working toward the Ph.D. degree.

His research interests include power electronics for photovoltaic systems, renewable energy, high-frequency/high-efficiency switched-mode power supplies, mixed-signal IC design, and motor drives.